Shear deformation behavior of the austenitic Σ3{112} twin boundary in NiTi shape memory alloy: An atomistic study

Zhibin Chen [a,b], Jiaxiang Shang [a,*], Yue Chen [b,*]

[a] *School of Materials Science and Engineering, Beihang University, Beijing 100191, China*

[b] *Department of Mechanical Engineering, The University of Hong Kong, Pokfulam Road, Hong Kong SAR, China*

* Corresponding author.

E-mail: *shangjx@buaa.edu.cn (J. Shang), yuechen@hku.hk (Y. Chen).*

Abstract: Molecular dynamics simulations are performed to study the deformation behavior of the austenitic Σ3{112} twin boundary (TB) of NiTi alloy under shear loading along different directions at 550 K, which is above the austenite finish temperature (535 K). The results show that the Σ3{112} TB retards the stress induced martensitic transformation (SIMT) when the TB is sheared along $[1\bar{1}0]$ but promotes the SIMT when it is sheared along $[11\bar{1}]$, which is perpendicular to $[1\bar{1}0]$. This direction dependence is related to the favorable transformation plane and the lattice correspondence between B2 austinite and B19′ martensite. Besides, the shear directions can be divided into four groups according to the martensite nucleation and growth processes. What is more, B19′ may nucleate firstly in the grain's interior or from the TB depending on the resolved shear stress. These findings are valuable for the design and application of NiTi alloy devices.

Keywords: shear deformation; grain boundary; molecular dynamics; shape memory alloy

1. Introduction

Owing to the extraordinary shape memory effect and superelasticity property resulted from a reversible phase transformation between cubic B2 austenite and monoclinic B19′ martensite, near-equiatomic NiTi shape memory alloys (SMAs) have been used extensively in biomedical, actuators and many other important industrial applications [1]. Another important property of B2 NiTi alloys is the anomalous ductility, which is attributed to the low elastic anisotropy and mechanical twinning systems, such as the $\{112\}_{B2}$ twinning which corresponds to $<110>_{B2}$ Σ3 symmetric tilt grain boundary (GB) [2-5]. The Σ value, calculated with $(h^2 + k^2 + l^2) / 2$, represents the reciprocal density of coinciding sites.

The energetics of $(\bar{2}11)$ twinning in B2 NiTi was established by a coupled shear and shuffle mechanism from first-principle calculations [6]. In addition, Yazdandoost and Mirzaeifar calculated the GB energies of the $<110>_{B2}$ symmetric tilt GBs from molecular dynamics (MD) simulations and found that the Σ3{112}<110> twin boundary (TB) possesses the smallest GB energy among the TBs with $\Sigma = 3^n$ (3, 9, 27 and so on) [7], which are important for the GB engineering of materials [5,8,9]. Another important aspect is the response of GBs under shear loading, which is critical for the comprehensive understanding of the mechanical behavior of polycrystalline materials, such as the GB-mediated plasticity [10]. The shear response of GBs in structural materials, such as bcc, fcc and hcp metals, have been studied extensively in both simulations and experiments, including pure sliding, migration, coupling motion (GB migration coupling with GB sliding) and dislocation emission from the GB [10-15]. The activated type of motion usually depends on the shear direction and temperature [10,11].

Although the austenitic Σ3{112}<110> TB has been observed extensively in deformed B2 NiTi or during the B2-B19′ martensitic transformation (MT) [4,5,9,16,17], few studies have been carried out to understand the role of austenitic Σ3{112}<110> TB on the MT. As reported by Ii et al. [5], this TB correlates with the {101} deformation twin in B19′ martensite. It was also reported that this TB can retard the thermally induced MT [18]. However, to the best of our knowledge, the response of GBs in austenitic NiTi under shear loading has not yet been reported. It still remains unclear whether the austenitic Σ3{112}<110> TB can retard the stress induced MT (SIMT) or not. Does the austenitic Σ3{112}<110> TB of NiTi shape memory alloy exhibit similar shear responses to those observed in structural materials? What is the relation between shear response and shear direction?

In the present study, we investigated the deformation behavior of the austenitic Σ3{112}<110> TB of NiTi alloy under shear loading along different directions parallel to the TB plane from MD simulations at 550 K, which is above the austenite finish (A_f) temperature. Interestingly, we find that the Σ3{112}<110> TB can either promote or retard the SIMT, depending on the shear direction. In addition, the shear directions can be divided into four groups according to the martensite nucleation and growth processes.

2. Method

MD simulation is a very powerful computational technique in investigating the evolution of structure and understanding of the underlying mechanisms, and it has been applied extensively to study the fundamental mechanisms of deformation behavior of materials in the past, including GB migration [10-14], phase transformation [18-23], and orientation-dependent pseudoelasticity [24]. In the current work, MD simulations are performed using the LAMMPS code [25] with a potential based on modified embedded-atom method (MEAM) [20] in the isothermal-isobaric (NPT) ensemble, where Nosé-Hoover thermostat and barostat [26,27] are used to control temperature and pressure, respectively, and the time step is 1 fs. Previous studies [21-24] have shown that this high-quality potential [20] can enable detailed analysis of the evolution of structure and understanding of the underlying mechanisms. For instance, Ko et al. [21] have investigated the temperature and stress induced transformations in nanocrystalline NiTi SMAs from MD simulation using the MEAM potential [20], and their results are consistent with available experimental observations, such as the decrease of the transformation temperature and the disappearance of the plateau in the stress-strain response with grain size decrease. Using the same MEAM potential [20], Sandoval et al. [22] studied the stability, structure, and suppression of the martensitic transition temperature by B19′ compound twin boundaries in NiTi and found that the results of MD simulations are very consistent with that of ab initio calculations.

The model of Σ3{112} TB with $[1\bar{1}0]$ tilt axis of B2 NiTi is shown in Fig. 1. The dimensions of the simulation models are approximately 180 × 180 × 205 Å (the dimensions slightly change for different directions to satisfy the periodicity). Periodic boundary conditions are applied along all directions. To obtain an initial TB structure with minimum energy, the in-plane rigid body translations and atoms deletion criteria are applied with a method similar to that applied in Ref. [7] and the Σ3{112} TB is equilibrated at 600 K for 200 picoseconds. Prior to shear loading, zero-stress transformation temperatures of the Σ3{112} TB are obtained from results of thermally induced MT. The temperature of the Σ3{112} TB is gradually decreased to 300 K and increased again to 600 K with a cooling and heating rates of 0.5 K ps^{-1}. During the MD simulations, the average potential energy (PE) is recorded to examine the phase transformations [18] and the A_f temperature is about 535 K (see Fig. 2). According to this result, the temperature is kept at 550 K to investigate the direction dependent shear response of the Σ3{112} TB.

During shear loading, two slabs at the top and bottom of the simulation cell are fixed (see Fig. 1) and the thickness of each slab is 10 Å which is twice of the cutoff radius of the MEAM potential [20]. The shear strain is applied by deforming the simulation cell as a whole at temperatures above A_f with a shear strain rate of 1×10^8 s^{-1}. The shear directions are aligned with the x or y axis of the simulation cell. Table 1 lists the shear directions and the included angles of the tilt axis $[1\bar{1}0]$ and shear direction. The stress components in directions other than the shear direction are set to zero to allow the relaxation of the Σ3{112} TB in these directions. Stress and temperature are calculated on the dynamic atoms between the two fixed slabs and the stress tensor is calculated by the standard virial expression [28].

The microstructures are characterized using common neighbor analysis (CNA) [29,30] as implemented in the OVITO program [31].

3. Results and discussion

3.1. Shear along the $[1\bar{1}0]$ direction

The stress-strain curves of the Σ3{112} TB and single crystal sheared along $[1\bar{1}0]$ (i.e., θ = 0°) at 550 K are shown in Fig. 3a. It is seen that the Σ3{112} TB undergoes elastic deformation before the stress reaches point A, and then two drops are observed in the loading stress-strain curve (see point A to B and C to D in Fig. 3a), corresponding to the MT occurred in the upper and lower grain (see Fig. 4a and b). It is worthy of note that the region near TB of the upper grain remains B2 austenite when martensite nucleates in the interior of the lower gain (see Fig. 4b). Similar martensite nucleation process during SIMT was also reported in other SMA [32]. As strain is increased to 15%, the upper and lower grains mostly transform to B19′ and the initial TB does not migrate (see the yellow atoms in Fig. 4c).

It can also be seen from Fig. 3a that the critical stress to trigger MT of the Σ3{112} TB is larger than that of single crystal, suggesting that the Σ3{112} TB retards the SIMT when the TB is sheared along $[1\bar{1}0]$. This is due to the facts that the atomic PE of the Σ3{112} TB is higher than that of single crystal and the TB cannot provide nucleation site. As can be seen from Fig. 3b, the atomic average PE of the Σ3{112} TB before shear loading is about -4.975 eV/atom, which is higher than that of single crystal (about -4.980 eV/atom). In addition, the reason why the B19′ nucleates in grains' interior instead of from TB may be that $(11\bar{1})_{B2}$ is not the favorable transformation plane. As reported in previous studies [20,33], the B19′ crystal structure can be considered as a monoclinic distortion and additional shuffling of Ni and Ti atoms on the $\{110\}_{B2}$ plane from the B2 structure. Following the notation used by Knowles and Smith [34], the transformation takes a tetragonal unit cell of the parent

B2 crystal structure into the monoclinic cell of the product B19′ structure (see Fig. 5). In an orthonormal basis parallel to the cube directions $[1\bar{1}0]$, [110] and [001], the deformation is represented by matrix

$$F = \frac{1}{a_0}\begin{bmatrix} b/\sqrt{2} & 0 & 0 \\ 0 & c\,sin\beta/\sqrt{2} & 0 \\ 0 & -c\,cos\beta/\sqrt{2} & a \end{bmatrix}, \tag{1}$$

where a_0 is the lattice parameter of the parent B2, and a, b, c and β are those of the monoclinic B19′ [34]. The shuffling of atoms in the unit cell can be ignored in the crystallographic theory of martensitic transformation [34]. In all of these six $\{110\}_{B2}$ planes, only $(1\bar{1}0)_{B2}$ of the upper grain is parallel to that of the lower grain. However, the $[1\bar{1}0]$ direction is the normal of $(1\bar{1}0)_{B2}$ plane, so the MT can only occur in other five $\{110\}_{B2}$ planes except $(1\bar{1}0)_{B2}$. If the B19′ nucleates directly from TB in these five $\{110\}_{B2}$ planes, it would result in an accumulation of local strains in the region near TB and introduce large local stress. Thus, the martensite nucleation is constrained to the grains' interior.

To analyze possible transformation planes, we define a vector m to show the shear stress in the $\{110\}_{B2}$ plane which transforms the B2 tetragonal unit cell to the B19′ monoclinic cell. In the first case, the included angle of the y axis of B2 tetragonal cell and m ($<m, y>$) is smaller than 90° and that of the z axis and m ($<m, z>$) is larger than 90° (see Fig. 5d), *i.e.*,

$$\cos <m, y> > 0 \text{ and } \cos <m, z> < 0. \tag{2}$$

In the second case, both $<m, y>$ and $<m, z>$ are larger than 90° (see Fig. 5e), *i.e.*,

$$\cos <m, y> < 0 \text{ and } \cos <m, z> < 0. \tag{3}$$

Based on these inequalities, the possible transformation planes of the lower grain are found to be $(101)_{B2}$ and $(\bar{1}01)_{B2}$ (see Table S1), and those of the upper grain are $(011)_{B2}$ and $(0\bar{1}1)_{B2}$ (see Table S2). By further comparing the atomic configurations of the enlarged views shown in Fig. 4g and h and the ideal $\{110\}_{B2}$ planes (Fig. S1), the transformation planes of the lower and upper grains are determined to be $(\bar{1}01)_{B2}$ and $(0\bar{1}1)_{B2}$, respectively.

Upon unloading, there are two rises in the unloading stress-strain curve of the Σ3{112} TB (see point E to F and G to H in Fig. 3a), which correspond to the completion of B19′-B2 transformation in lower and upper grain (see Fig. 4d-f). After the completion of B19′-B2 transformation, the stress-strain curves of unloading of the Σ3{112} TB and single crystal overlap with those of loading and the shear strain recovers to zero, suggesting the superelasticity behavior. It is noted that the superelastic strain obtained in our simulation is larger than that observed in experiments (about 8%); this may be related to the random dislocations, second phases (e.g., R-phase and Ni_4Ti_3 precipitates), and various grain boundaries in NiTi SMAs, which introduce plastic deformation during MT. Our Σ3{112} TB model is built without any second phase or random dislocation in the interior of the upper and lower crystals; the initial TB structure with minimum energy is obtained by applying the in-plane rigid body translation method similar to Ref. [7]. The single crystal model is also built without any second phase or dislocation, and it is equilibrated at 600 K without external pressure before shear loading. It can also be seen from the stress-strain curves shown in Fig. 3 that no obvious plastic deformation is introduced in the Σ3{112} TB model and the single crystal when strain reaches 15%; this result can be further confirmed by the atomic configurations shown in Fig. 4 and Fig. S2.

3.2. Shear along the $[11\bar{1}]$ direction

The stress-strain curves of the Σ3{112} TB and single crystal sheared along $[11\bar{1}]$ (i.e., θ = 90°) at 550 K are shown in Fig. 6. The loading stress-strain curve of the Σ3{112} TB exhibits a sigmoidal shape behavior, where the stress plateau is caused by the SIMT. It is worth noting that the initial TB transforms into a phase boundary (PB) without relative rigid-body sliding along the TB plane (see Fig. 7a), indicating that the Σ3{112} TB acts as a nucleation site when the TB is sheared along $[11\bar{1}]$. The downward migration of PB is accompanied by the B2-B19′ transformation. As further deformation imposed, the entire lower grain transforms to B19′ while the upper grain remains austenite (see Fig. 7b). Similar martensite nucleation and growth processes during SIMT were also observed in other SMA [32].

It can also be seen from Fig. 6 that the stress to trigger MT of the Σ3{112} TB is lower than that of the single crystal, which means that the Σ3{112} TB promotes the SIMT when the TB is sheared along $[11\bar{1}]$. This may be because the $[11\bar{1}]$ direction lies in the $(1\bar{1}0)_{B2}$ plane, which is one of the favorable $\{110\}_{B2}$ transformation planes, and $(1\bar{1}0)_{B2}$ of the upper grain is parallel to that of the lower grain. The possible transformation plane of lower grain is found to be $(1\bar{1}0)_{B2}$ and those of the upper grain are $(101)_{B2}$ and $(011)_{B2}$ (see Table S3 and Table S4). In addition, it has been reported in an experimental work [5] that the $\{101\}_{B19'}$ deformation twin correlates with the Σ3{112}<110> TB of B2 NiTi. As shown in Fig. 7c, the orientation relationship between B19′ and B2 is as follows:

$$[100]_{B19'}\ 14.9^{\circ}\ \text{from}\ [001]_{B2},$$

$$[010]_{B19'} \parallel [\bar{1}10]_{B2},$$

$$[001]_{B19'}\ 6.7^{\circ}\ \text{from}\ [\bar{1}\bar{1}0]_{B2}.$$

As can be confirmed by the lattice correspondence

$$\begin{pmatrix} 0 & 0 & 1 \\ -1 & 1 & 0 \\ -1 & -1 & 0 \end{pmatrix} \begin{pmatrix} 1 \\ 1 \\ 2 \end{pmatrix}_{B2} = 2 \begin{pmatrix} 1 \\ 0 \\ -1 \end{pmatrix}_{B19'}, \tag{4}$$

$(10\bar{1})_{B19'}$ is parallel to $(112)_{B2}$ (see the magenta and black dashed lines in Fig. 7c). Therefore, the Σ3{112} TB can act as a nucleation site of martensite and does not result in accumulation of local strains in the region near TB when B19′ nucleates and grows downward from TB. Thus, the phenomenon that the Σ3{112} TB promotes the SIMT when the TB is sheared along $[11\bar{1}]$ is rationalized.

For the upper grain, no transformation is observed even at shear strain ε = 15%. It is known that the possible transformation planes of the upper grain are $(011)_{B2}$ and $(101)_{B2}$. If the MT occurred in these two planes, the B19′ martensite can only nucleate in the upper grain's interior, because $(1\bar{1}0)_{B2}$ of the upper grain is not a possible transformation plane (see Table S4), *i.e.*, the TB cannot act as a nucleation site of B19′ martensite. When the Σ3{112} TB is sheared along $[1\bar{1}0]$, B19′ nucleates firstly in the upper grain's interior with a transformation plane of $(0\bar{1}1)_{B2}$, and the critical shear stress to trigger the MT in upper grain is 1.30 GPa, of which the absolute value of the resolved stress to [100] in the $(0\bar{1}1)_{B2}$ plane is 0.92 GPa. For the Σ3{112} TB sheared along $[11\bar{1}]$, the shear stress at strain ε = 15.0% is 1.87 GPa. During shear loading, atoms in the upper grain move uniformly, and the included angle between the [100] axis and the projection vector of shear direction $[11\bar{1}]$ in the $(011)_{B2}$ plane decreases with increasing strain (see Fig. S3); the included angle between the [010] axis and the projection vector of shear direction $[11\bar{1}]$ in the $(101)_{B2}$ plane also decreases with increasing strain (see Fig. S4). When ε = 15.0%, the included angles in $(011)_{B2}$ and $(101)_{B2}$ planes are about 114.0^{o} and 115^{o}, respectively. Therefore, the absolute values of resolved stress of 1.87 GPa to the [100] in $(011)_{B2}$ and [010] in $(101)_{B2}$ planes are 0.76 GPa and 0.79 GPa, respectively. Because both of these resolved stresses are both smaller than 0.92 GPa, there is no transformation in the upper grain when the Σ3{112} TB is sheared along $[11\bar{1}]$.

It can also be seen from the stress-strain curves (Fig. 6) and the atomic configurations (Fig. 7 and Fig. S2) that the B19′ martensite and the retained B2 austenite only undergo elastic deformation and do not show plastic deformation even when strain reaches 15%. During unloading, the B19′ phase near the lower border of the Σ3{112} TB transforms back into B2 firstly (see Fig. 7d). After the completion of B19′-B2 transformation, the stress-strain curves of unloading of the Σ3{112} TB and single crystal overlap with those of loading and the shear strain recovers to zero (see Fig. 6). It can also be seen from

Fig. 6 that the mechanical hysteresis of the Σ3{112} TB is smaller than that of single crystal, which may shed light on the design of actuators requiring superelasticity and low hysteresis.

3.3. Shear along directions between $[1\bar{1}0]$ and $[11\bar{1}]$

To study the effect of shear direction on the deformation behavior of the Σ3{112} TB, we conduct a series of simulations with shear directions between $[1\bar{1}0]$ and $[11\bar{1}]$ (i.e., $0° < \theta < 90°$) at 550 K. The stress-strain curves of the Σ3{112} TB under shear loading along different directions are shown in Fig. 8, and the representative atomic configurations are shown in Fig. 9. As can be seen from Fig. 8a, the curve of $\theta = 0^o$ or 19.3^o has two stress drops which correspond to the MT in the upper and lower grains. It can also be seen from Fig. 4 and Fig. 9a that the B2-B19′ MT occurs firstly in the upper grain and then in the lower grain. For $\theta = 31.5^o$, the curve shape before the first stress drop is similar to those of 0^o and 19.3^o, but the phase transformation process is the same with that of 39.2^o (see Fig. 9b and c), during which the B2-B19′ transformation occurs firstly in the lower grain and then in the upper grain before the MT finishes in the lower grain. When $\theta = 50.8^o$ or 61.4^o, there is a stress plateau before the stress suddenly drops (see Fig. 8a), and it can be found from Fig. 9d and e that the lower gain completes the B2-B19′ transformation before the MT occurs in the upper grain. In addition, the curve of 70.7^o or 90^o exhibits a sigmoidal shape behavior, where the stress plateau is caused by the SIMT (see Fig. 8a), and it is found from Fig. 7 and Fig. 9f that MT only occurs in the lower grain.

It is interesting that B19′ starts nucleating in the interior of the upper grain when $0^o \leq \theta \leq 19.3^o$ and from the TB when $31.5^o \leq \theta \leq 90^o$. The direction dependent nucleation can be explained by the resolved shear stress. The first critical shear stress τ_c to trigger the MT and the first transformation plane (see Fig. 4, Fig. 7 and Fig. 10) are summarized in Table 1. It is found that the first phase transformation plane is $(0\bar{1}1)_{B2}$ when $0^o \leq \theta \leq 19.3^o$ and $(1\bar{1}0)_{B2}$ when $31.5^o \leq \theta \leq 90^o$. Because $[1\bar{1}0]$ is perpendicular to $[11\bar{1}]$ and their phase transformation planes are different, the τ_c of intermediate directions can be resolved to these two orientations. It can be seen from Table 1 that the resolved stress of τ_c to $[11\bar{1}]$ (τ-$[11\bar{1}]$) is close to 0.55 GPa when $31.5^o \leq \theta < 90^o$, while the resolved stress of τ_c to axis $[1\bar{1}0]$ (τ-$[1\bar{1}0]$) is smaller than 1.30 GPa and 1.06 GPa (the stress plateau after the first stress drop when $\theta = 0^o$). Thus, the fact that the B19′ phase nucleates firstly from TB when $31.5^o \leq \theta < 90^o$ is rationalized. For the $\Sigma3\{112\}$ TB sheared along $[9\ \bar{5}\ \bar{2}]$ ($\theta = 19.3^o$), its τ-$[11\bar{1}]$ (= 0.41 GPa) is smaller than 0.55 GPa, but its τ-$[1\bar{1}0]$ (= 1.18 GPa) is larger than 1.06 GPa though a little smaller than 1.30 GPa, so the nucleation of B19′ phase in the interior of the upper grain is reasonable. The resolved stress of the first τ_c is also shown in Fig. 8b. To certain extend, we may infer from these resolved stresses and the phase transformation process shown in Fig. 4, Fig. 7 and Fig. 9 that these shear directions can be divided into four groups: (1) $0^o \leq \theta < 22.5^o$, (2) $22.5^o \leq \theta < 45^o$, (3) $45^o \leq \theta < 67.5^o$, and (4) $67.5^o \leq \theta \leq 90^o$.

It can also be seen from Fig. 4 and Fig. 10 that the transformation plane of upper grain is $(0\bar{1}1)_{B2}$ when the $\Sigma3\{112\}$ TB is sheared along directions with $\theta \leq 61.4^o$. Similar to the $\Sigma3\{112\}$ TB sheared along $[11\bar{1}]$ ($\theta = 90^o$), there is no MT observed in the upper grain when the $\Sigma3\{112\}$ TB is sheared along $[10\ 4\ \bar{7}]$ ($\theta = 70.7^o$). When $\varepsilon = 15.0\%$, the stress of the $\Sigma3\{112\}$ TB sheared along $[10\ 4\ \bar{7}]$ is 2.06 GPa, of which the resolved stresses to $[1\bar{1}0]$ and $[11\bar{1}]$ are 0.68 and 1.94 GPa, respectively. Because τ-$[1\bar{1}0]$, which is equal to 0.68 GPa, is smaller than 1.30 GPa (the critical τ_c to trigger MT in the upper grain's interior when the $\Sigma3\{112\}$ TB is sheared along $[1\bar{1}0]$ direction), MT cannot occur in the $(0\bar{1}1)_{B2}$ plane of the upper grain. Moreover, τ-$[11\bar{1}]$ (1.94 GPa) is a little larger than 1.87 GPa, the shear stress at $\varepsilon = 15.0\%$ when the $\Sigma3\{112\}$ TB is sheared along $[11\bar{1}]$. <u>Because the included angle</u>

between the [100] axis and the projection vector of shear direction [11¯,1] in the $(011)_{B2}$ plane and that between the [010] axis and the projection vector of shear direction [11¯,1] in the $(101)_{B2}$ plane are both about 113.0^{o} when shear strain is equal to 15% (see Fig. S5), the absolute values of the resolved stress of 1.94 GPa to [100] in $(011)_{B2}$ and [010] in $(101)_{B2}$ are both about 0.76 GPa, which is smaller than 0.92 GPa (the absolute value of the resolved stress of 1.30 GPa to [100] in the (0¯,11)$_{B2}$ plane). Thus, MT also cannot occur in the $(011)_{B2}$ or $(101)_{B2}$ plane of the upper grain. After all, no transformation is observed in the upper grain when the Σ3{112} TB is sheared along $[10\ 4\ \bar{7}]$.

4. Conclusions

In this work, we have investigated the deformation behavior of the austenitic Σ3{112} TB in NiTi alloy under shear loading from MD simulations, the main conclusions are as follows:

(1) The results at 550 K show that the Σ3{112} TB promotes the SIMT when the TB is sheared along $[11\bar{1}]$ but retards the SIMT when the TB is sheared along $[1\bar{1}0]$. This direction dependence is related to the favorable transformation plane and the lattice correspondence between B2 and B19′.

(2) The shear directions can be divided into four groups according to the martensite nucleation and growth processes: (1) $0^o \le \theta < 22.5^o$, (2) $22.5^o \le \theta < 45^o$, (3) $45^o \le \theta < 67.5^o$, and (4) $67.5^o \le \theta \le 90^o$.

(3) B19′ may nucleate firstly in the grain’s interior or from the TB depending on the resolved shear stress.

Declaration of Competing Interest

The authors declared that there is no conflict of interest.

Acknowledgments

The authors acknowledge the financial support from the National Natural Science Foundation of China (Grant No. 51371017). The computations were performed using research computing facilities offered by ITS, HKU.

Appendix A. Supplementary material

References

[1] J. Mohd Jani, M. Leary, A. Subic, M.A. Gibson, A review of shape memory alloy research, applications and opportunities, Mater. Des., 56 (2014) 1078-1113.

[2] S. Miyazaki, K. Otsuka, Y. Suzuki, Transformation pseudoelasticity and deformation behavior in a Ti-50.6at% Ni alloy, Scr. Metall., 15 (1981) 287-292.

[3] K. Otsuka, X. Ren, Physical metallurgy of Ti–Ni-based shape memory alloys, Prog. Mater. Sci., 50 (2005) 511-678.

[4] M. Nishida, M. Matsuda, T. Fujimoto, K. Tanka, A. Kakisaka, H. Nakashima, Crystallography of deformation twin boundaries in a B2 type Ti–Ni alloy, Mater. Sci. Eng., A, 438-440 (2006) 495-499.

[5] S. Ii, M. Matsuda, T. Matsui, T. Fujimoto, A. Kakisaka, T. Kikutake, S. Tsurekawa, K.-i. Ikeda, M. Nishida, Controlling grain boundary character distribution of high-temperature B2 phase in Ti–Ni–Fe alloy, Intermetallics, 31 (2012) 65-71.

[6] T. Ezaz, H. Sehitoglu, Coupled shear and shuffle modes during twin growth in B2-NiTi, Appl. Phys. Lett., 98 (2011) 241906.

[7] F. Yazdandoost, R. Mirzaeifar, Tilt grain boundaries energy and structure in NiTi alloys, Comput. Mater. Sci., 131 (2017) 108-119.

[8] V. Randle, Twinning-related grain boundary engineering, Acta Mater., 52 (2004) 4067-4081.

[9] I. Karaman, A.V. Kulkarni, Z.P. Luo, Transformation behaviour and unusual twinning in a NiTi shape memory alloy ausformed using equal channel angular extrusion, Philos. Mag., 85 (2005) 1729-1745.

[10] L. Wan, S. Wang, Shear response of the Σ9⟨110⟩{221} symmetric tilt grain boundary in fcc metals studied by atomistic simulation methods, Phys. Rev. B, 82 (2010) 214112.

[11] B.-W. Huang, J.-X. Shang, Z.-H. Liu, Y. Chen, Atomic simulation of bcc niobium Σ5<001>{310} grain boundary under shear deformation, Acta Mater., 77 (2014) 258-268.

[12] C. Molteni, N. Marzari, M.C. Payne, V. Heine, Sliding mechanisms in aluminum grain boundaries, Phys. Rev. Lett., 79 (1997) 869-872.

[13] J.W. Cahn, Y. Mishin, A. Suzuki, Coupling grain boundary motion to shear deformation, Acta Mater., 54 (2006) 4953-4975.

[14] D.E. Spearot, L. Capolungo, C.N. Tomé, Shear-driven motion of Mg {10-12} twin boundaries via disconnection terrace nucleation, growth, and coalescence, Phys. Rev. Materials, 3 (2019) 053606.

[15] D.A. Molodov, V.A. Ivanov, G. Gottstein, Low angle tilt boundary migration coupled to shear deformation, Acta Mater., 55 (2007) 1843-1848.

[16] E. Goo, T. Duerig, K. Melton, R. Sinclair, Mechanical twinning in $Ti_{50}Ni_{47}Fe_3$ and $Ti_{49}Ni_{51}$ alloys, Acta Metall., 33 (1985) 1725-1733.

[17] A.N. Tyumentsev, N.S. Surikova, I.Y. Litovchenko, Y.P. Pinzhin, A.D. Korotaev, O.V. Lysenko, Mechanism of deformation and crystal lattice reorientation in strain localization bands and deformation twins of the B2 phase of titanium nickelide, Acta Mater., 52 (2004) 2067-2074.

[18] S.-J. Qin, J.-X. Shang, F.-H. Wang, Y. Chen, Symmetrical tilt grain boundary engineering of NiTi shape memory alloy: An atomistic insight, Mater. Des., 137 (2018) 361-370.

[19] S. Qin, J. Shang, X. Wang, F. Wang, S. Qin, J. Shang, X. Wang, F. Wang, Effects of B2/B19' phase boundary on thermally induced phase transition in NiTi: An atomistic study, Appl. Surf. Sci., 353 (2015) 1052-1060.

[20] W.-S. Ko, B. Grabowski, J. Neugebauer, Development and application of a Ni-Ti interatomic potential with high predictive accuracy of the martensitic phase transition, Phys. Rev. B, 92 (2015) 134107

[21] W.-S. Ko, S.B. Maisel, B. Grabowski, J.B. Jeon, J. Neugebauer, Atomic scale processes of phase transformations in nanocrystalline NiTi shape-memory alloys, Acta Mater., 123 (2017) 90-101.

[22] L. Sandoval, J.B. Haskins, J.W. Lawson, Stability, structure, and suppression of the martensitic transition temperature by B19′ compound twins in NiTi: ab initio and classical simulations, Acta Mater., 154 (2018) 182-189.

[23] B. Wang, G. Kang, Q. Kan, W. Wu, K. Zhou, C. Yu, Atomistic study on the super-elasticity of nanocrystalline NiTi shape memory alloy subjected to a cyclic deformation, Comput. Mater. Sci., 152 (2018) 85-92.

[24] P. Srinivasan, L. Nicola, A. Simone, Atomistic modeling of the orientation-dependent pseudoelasticity in NiTi: Tension, compression, and bending, Comput. Mater. Sci., 154 (2018) 25-36.

[25] S. Plimpton, Fast Parallel Algorithms for Short-Range Molecular Dynamics, J. Comput. Phys., 117 (1995) 1-19.

[26] S. Nosé, A unified formulation of the constant temperature molecular dynamics methods, J. Chem. Phys., 81 (1984) 511-519.

[27] W.G. Hoover, Canonical dynamics: Equilibrium phase-space distributions, Phys. Rev. A, 31 (1985) 1695-1697.

[28] A.P. Thompson, S.J. Plimpton, W. Mattson, General formulation of pressure and stress tensor for arbitrary many-body interaction potentials under periodic boundary conditions, J. Chem. Phys., 131 (2009) 154107.

[29] A. Stukowski, Structure identification methods for atomistic simulations of crystalline materials, Model. Simul. Mater. Sci. Eng., 20 (2012) 045021.

[30] J.D. Honeycutt, H.C. Andersen, Molecular dynamics study of melting and freezing of small Lennard-Jones clusters, J. Phys. Chem., 91 (1987) 4950-4963.

[31] S. Alexander, Visualization and analysis of atomistic simulation data with OVITO–the Open Visualization Tool, Model. Simul. Mater. Sci. Eng., 18 (2010) 015012.

[32] S.M. Ueland, C.A. Schuh, Grain boundary and triple junction constraints during martensitic transformation in shape memory alloys, J. Appl. Phys., 114 (2013) 053503.

[33] K. Otsuka, T. Sawamura, K. Shimizu, Crystal structure and internal defects of equiatomic TiNi martensite, Physica Status Solidi A, 5 (1971) 457-470.

[34] K.M. Knowles, D.A. Smith, The crystallography of the martensitic transformation in equiatomic nickel-titanium, Acta Metall., 29 (1981) 101-110.

Tables

Table 1. First critical shear stress τ_c to induce SIMT, first nucleation site, and first transformation plane of the Σ3{112} TB sheared along different directions at 550 K. θ is the included angle of the tilt axis $[1\bar{1}0]$ and the shear direction. τ-$[1\bar{1}0]$ and τ-$[11\bar{1}]$ are the resolved stresses of τ_c to $[1\bar{1}0]$ and $[11\bar{1}]$ directions, respectively.

θ	0°	19.3°	31.5°	39.2°	50.8°	61.4°	70.7°	90°
orientation	$[1\ \bar{1}\ 0]$	$[9\ \bar{5}\ \bar{2}]$	$[3\ \bar{1}\ \bar{1}]$	$[5\ \bar{1}\ \bar{2}]$	$[2\ 0\ \bar{1}]$	$[5\ 1\ \bar{3}]$	$[10\ 4\ \bar{7}]$	$[1\ 1\ \bar{1}]$
nucleation site	interior	interior	TB	TB	TB	TB	TB	TB
transformation plane	$(0\bar{1}1)_{B2}$	$(0\bar{1}1)_{B2}$	$(1\bar{1}0)_{B2}$	$(1\bar{1}0)_{B2}$	$(1\bar{1}0)_{B2}$	$(1\bar{1}0)_{B2}$	$(1\bar{1}0)_{B2}$	$(1\bar{1}0)_{B2}$
τ_c (GPa)	1.30	1.25	1.03	0.92	0.72	0.65	0.60	0.55
τ-$[1\bar{1}0]$ (GPa)	1.30	1.18	0.88	0.71	0.46	0.31	0.20	0
τ-$[11\bar{1}]$ (GPa)	0	0.41	0.54	0.58	0.56	0.57	0.57	0.55

Figure captions

Fig. 1. Schematic illustration of the model and initial structural unit of the Σ3(112)$[1\bar{1}0]$ TB. The crystallographic directions are defined with reference to the lower crystal. The z axis, which is also the normal of the TB plane, is aligned with [112]. The upper crystal is created by a 180° rotation of the lower crystal around the z axis. θ is the included angle of the tilt axis $[1\bar{1}0]$ and shear direction X′. Ni and Ti atoms are shown by green and gray spheres, respectively.

Fig. 2. Average potential energy (PE) as a function of temperature during the cooling and heating processes. The martensite start (M_s) and finish (M_f) temperatures are indicated by the black arrows. The austenite start (A_s) and finish (A_f) temperatures are indicated by the blue arrows.

Fig. 3. (a) Stress-strain curves of the Σ3{112} TB and single crystal sheared along $[1\bar{1}0]$ (i.e., θ = 0°) at 550 K. (b) Average potential energies (PEs) of the Σ3{112} TB and single crystal under shear loading at 550 K.

Fig. 4. Atomic configurations of the Σ3{112} TB sheard along $[1\bar{1}0]$ at 550 K. Only the atoms in dynamic region are displayed. Atoms in (a)-(f) are colored according to the CNA pattern. Blue, red, and gray atoms correspond to the B2 austenite, the B19′ martensite, and the TB, respectively. Some atoms of B2 or B19′ phase may be displayed in gray due to the thermal perturbation. Yellow atoms correspond to those with scaled x coordinates (from 0 to 1) between 0.48 and 0.52 when shear strain $\varepsilon = 0.0\%$; their atomic identifier (ID) numbers are stored to track their positions. The black dashed line marks the initial TB plane. Panel (g) and (h) are the enlarged views of the white square regions in panel (a) and (b), respectively. Ni and Ti atoms in (g) and (h) are shown by green and gray spheres, respectively. The blue rectangles and red parallelograms indicate the unit cells of B2 and B19′, respectively.

Fig. 5. (a) Schematic diagram of transformation from B2 austenite to B19′ martensite. (b) Tetragonal cell of B2 austenite. Ni and Ti atoms are shown with gray and blue spheres, respectively. (c) Monoclinic cell of B19′ martensite; (d) and (e) represent the two cases in which the shear stress *m* in the $\{110\}_{B2}$ plane transforms the B2 tetragonal cell to the B19′ monoclinic cell.

Fig. 6. Stress-strain curves of the Σ3{112} TB and single crystal sheared along $[11\bar{1}]$ (i.e., θ = 90°) at 550 K.

Fig. 7. Atomic configurations of the Σ3{112} TB sheard along $[11\bar{1}]$ at 550 K. Only the atoms in dynamic region are displayed. Atoms in panel (a), (b), (d) and (e) are colored according to the CNA pattern. Blue, red, and gray atoms correspond to the B2 austenite ($\beta = 90^o$), the B19′ martensite ($\beta \approx 98^o$), and the TB (PB), respectively. Some atoms of B2 or B19′ phase may be displayed in gray due to the thermal perturbation. Yellow atoms correspond to those with scaled y coordinates (from 0 to 1)

between 0.48 and 0.52 when shear strain ε = 0.0%; their atomic ID numbers are stored to track their positions. (c) Enlarged view of the white square region in panel (b). Atoms in panel (c) are colored according to their types (Ni and Ti atoms are shown in green and gray, respectively). The black dashed line marks the PB plane, which is also the $(112)_{B2}$. The magenta dashed line marks the $(10\bar{1})_{B19'}$. The orange dashed lines show the initial B2 orientations which are used to measure the angle between $[100]_{B19'}$ and $[00\bar{1}]_{B2}$ and the angle between $[001]_{B19'}$ and $[110]_{B2}$.

Fig. 8. (a) Stress-strain curves of the Σ3{112} TB under shear loading at 550 K along different directions (0° ≤ θ ≤ 90°). (b) First critical shear stress to induce the B2-B19′ transformation and the corresponding resolved stresses. (c) Shear directions and their included angles.

Fig. 9. Atomic configurations of the Σ3{112} TB sheared at 550 K along different directions (0° < θ < 90°). Only the atoms in dynamic region are displayed. Atoms are colored according to the CNA pattern. Blue, red, and gray atoms correspond to the B2 austenite, the B19′ martensite, and the TB (PB), respectively. Some atoms of B2 or B19′ phase may be displayed in gray due to the thermal perturbation.

Fig. 10. Transformation planes of the Σ3{112} TB sheared along diferrent directions at 550 K. Atoms are colored according to the CNA pattern. Blue, red, and gray atoms correspond to the B2 austenite, the B19′ martensite, and the TB (PB), respectively. Some atoms of B2 or B19′ phase may be displayed in gray due to the thermal perturbation.

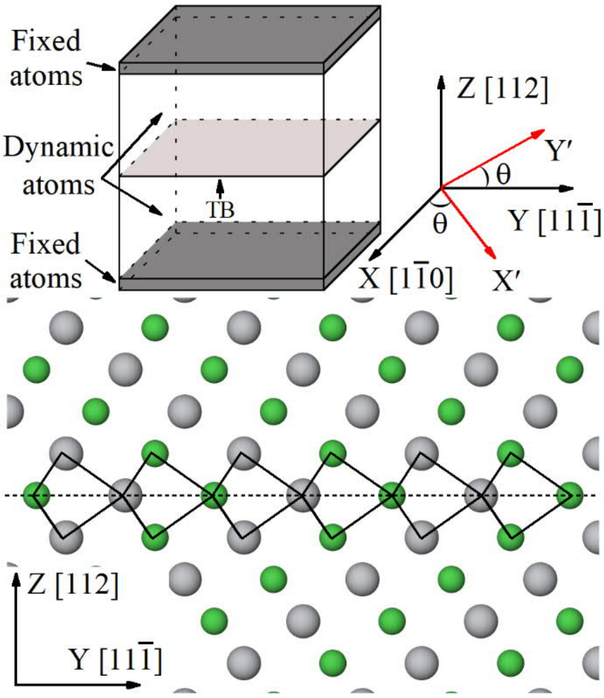
Fixed atoms
Dynamic atoms
TB
Fixed atoms
Z [112]
Y′
θ
Y [11$\bar{1}$]
θ
X [1$\bar{1}$0]
X′
Z [112]
Y [11$\bar{1}$]

Fig. 1

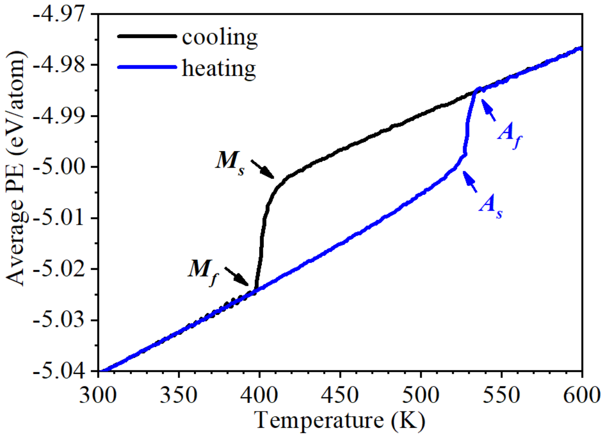
-4.97
-4.98
-4.99
-5.00
-5.01
-5.02
-5.03
-5.04
Average PE (eV/atom)
300
350
400
450
500
550
600
Temperature (K)
cooling
heating
M_s
M_f
A_f
A_s

Fig. 2

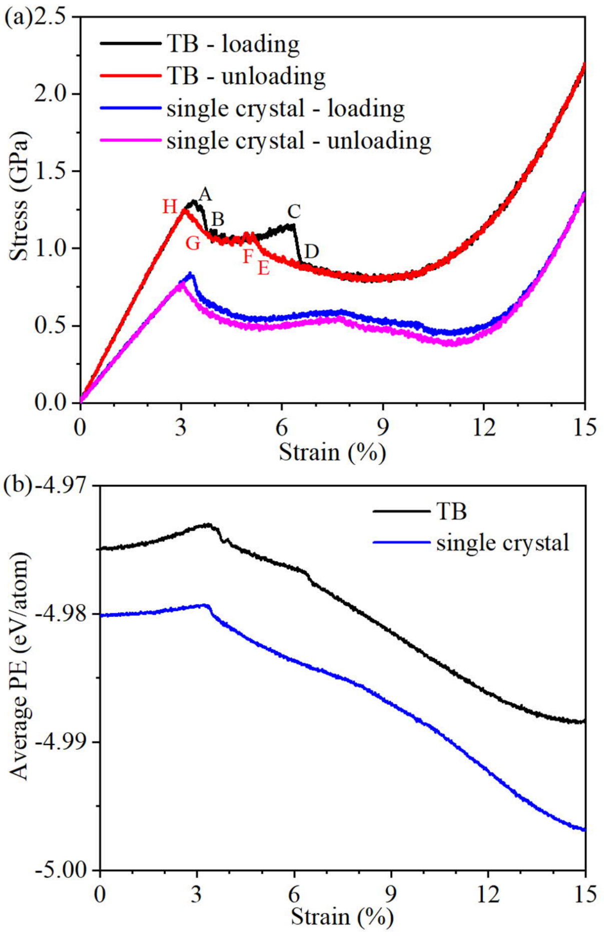
(a)
2.5
2.0
1.5
1.0
0.5
0.0
Stress (GPa)
TB - loading
TB - unloading
single crystal - loading
single crystal - unloading
A
B
C
D
H
G
F
E
0
3
6
9
12
15
Strain (%)
(b)
-4.97
-4.98
-4.99
-5.00
Average PE (eV/atom)
TB
single crystal
0
3
6
9
12
15
Strain (%)

Fig. 3

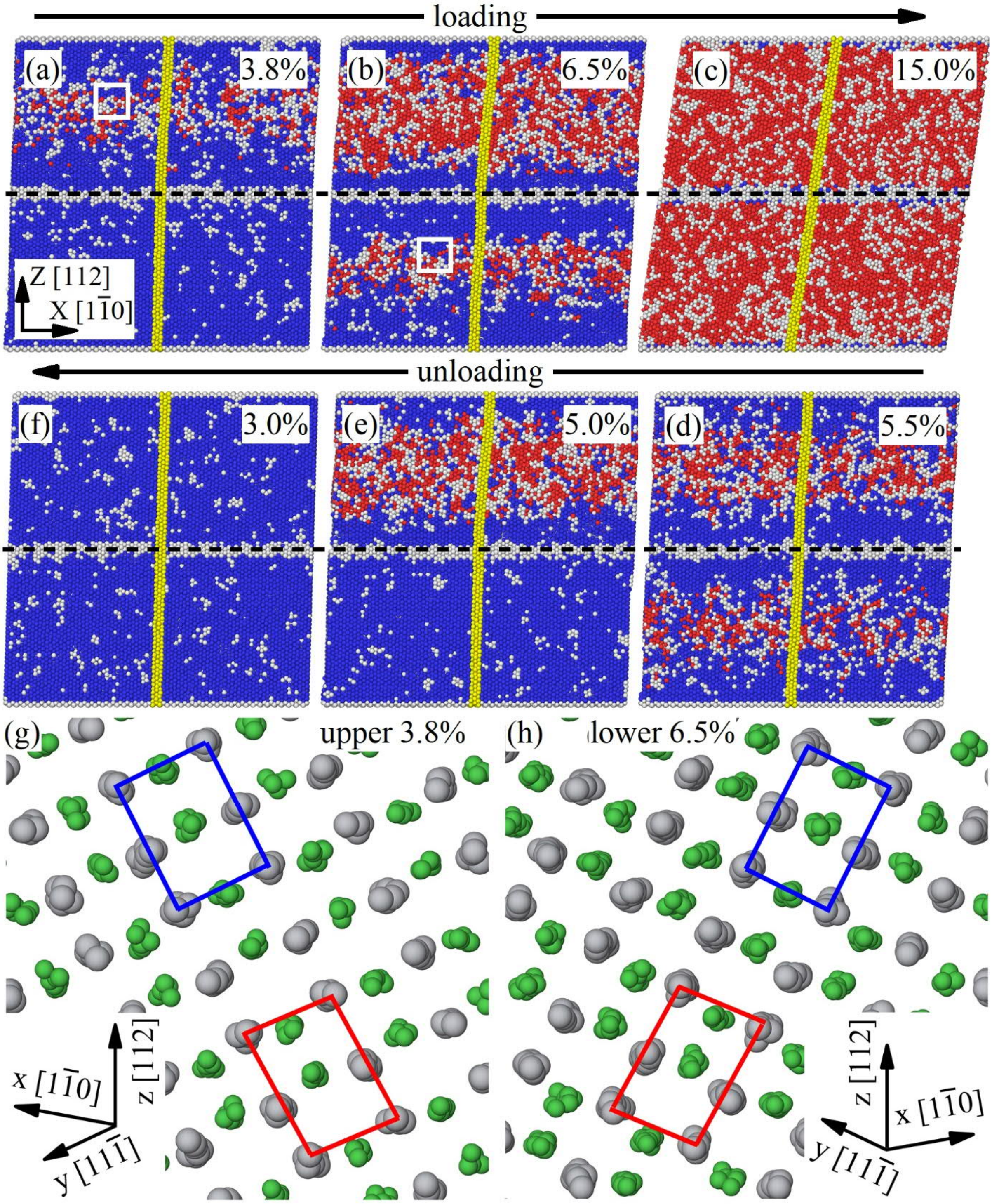
loading
unloading
(a)
3.8%
(b)
6.5%
(c)
15.0%
(f)
3.0%
(e)
5.0%
(d)
5.5%
Z [112]
X [1$\bar{1}$0]
(g)
upper 3.8%
(h)
lower 6.5%
x [1$\bar{1}$0]
z [112]
y [11$\bar{1}$]

Fig. 4

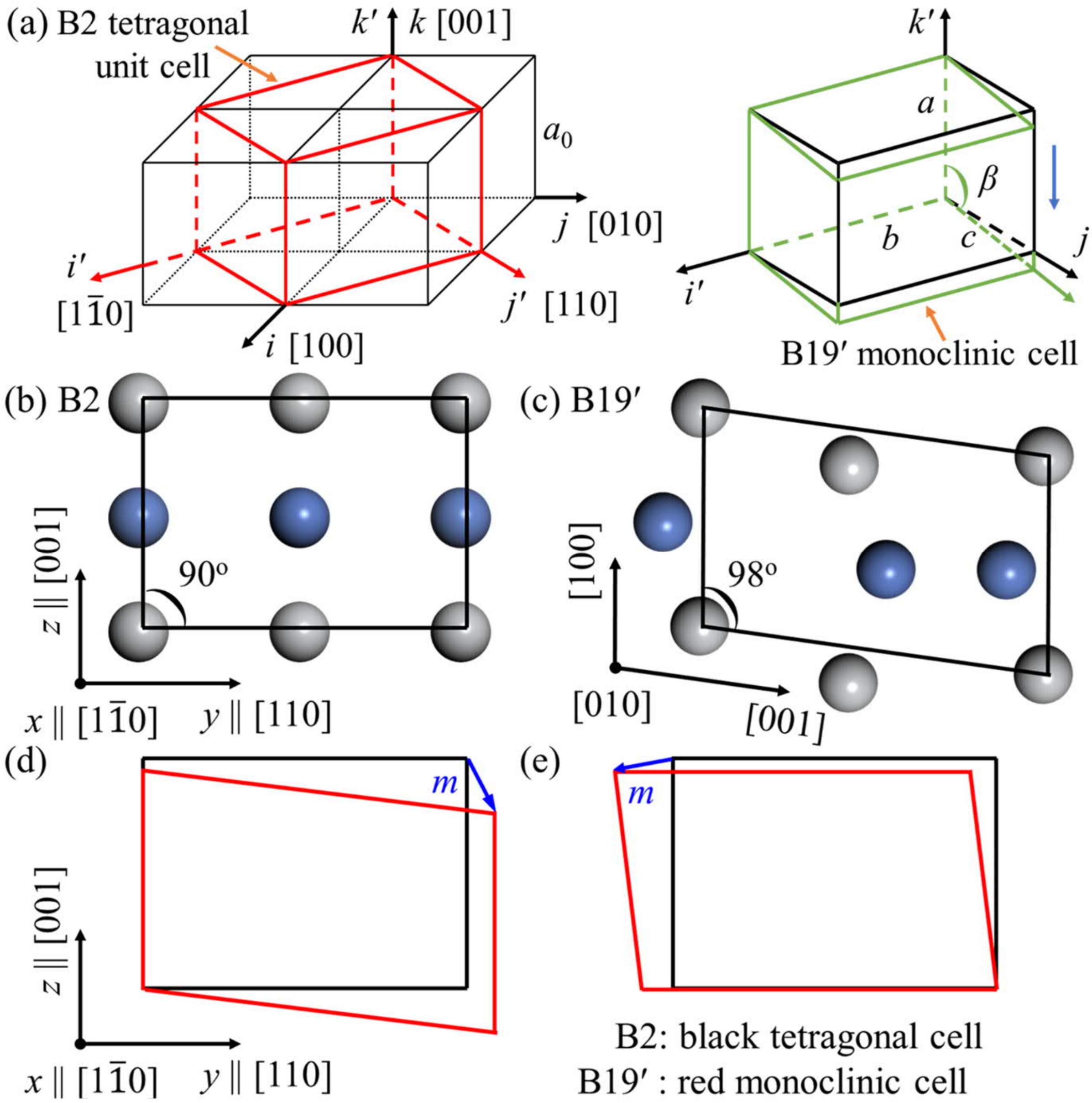
(a) B2 tetragonal unit cell
k′
k [001]
a₀
j [010]
i′
[1$\bar{1}$0]
j′ [110]
i [100]
k′
a
β
b
c
j′
i′
B19′ monoclinic cell
(b) B2
90°
z ∥ [001]
x ∥ [1$\bar{1}$0]
y ∥ [110]
(c) B19′
98°
[100]
[010]
[001]
(d)
m
z ∥ [001]
x ∥ [1$\bar{1}$0]
y ∥ [110]
(e)
m
B2: black tetragonal cell
B19′ : red monoclinic cell

Fig. 5

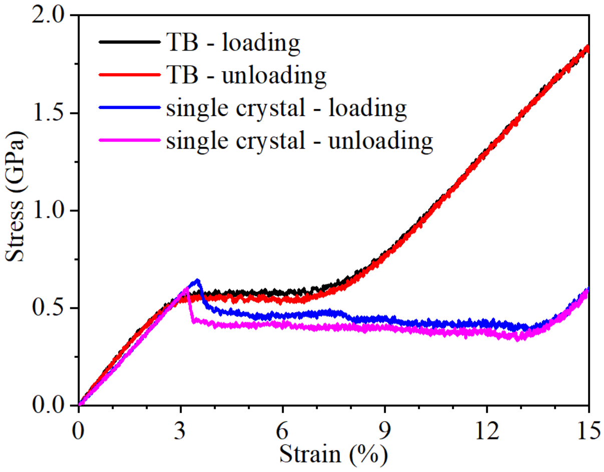
2.0
1.5
1.0
0.5
0.0
Stress (GPa)
0
3
6
9
12
15
Strain (%)
TB - loading
TB - unloading
single crystal - loading
single crystal - unloading

Fig. 6

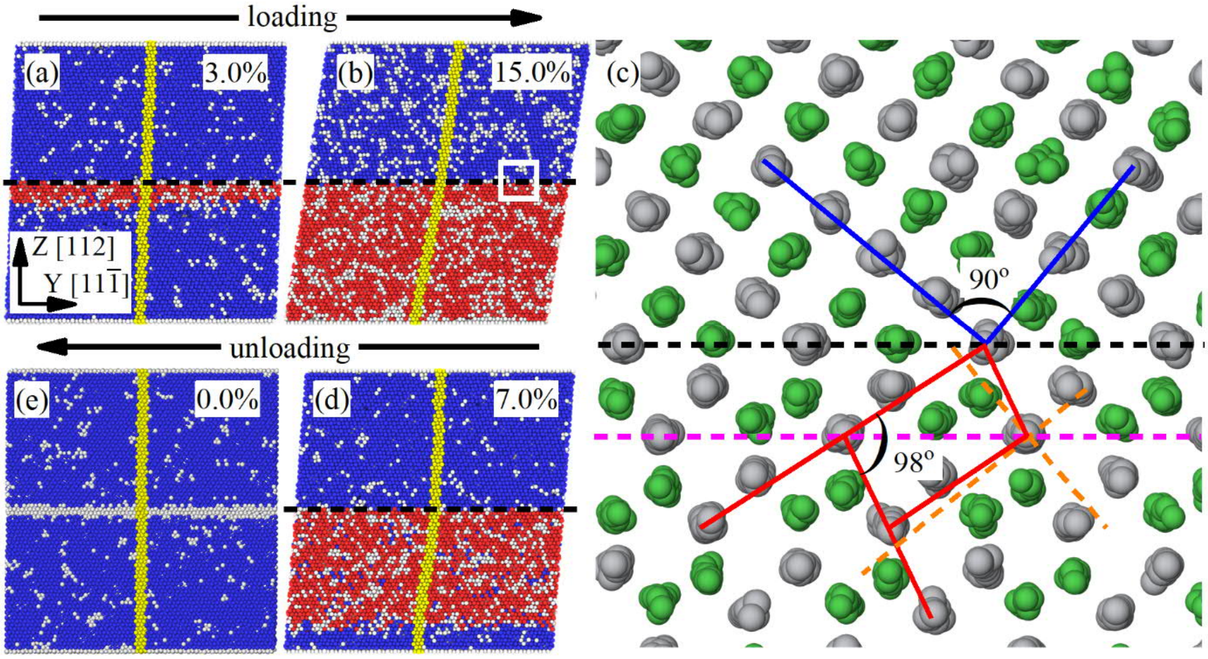

Fig. 7

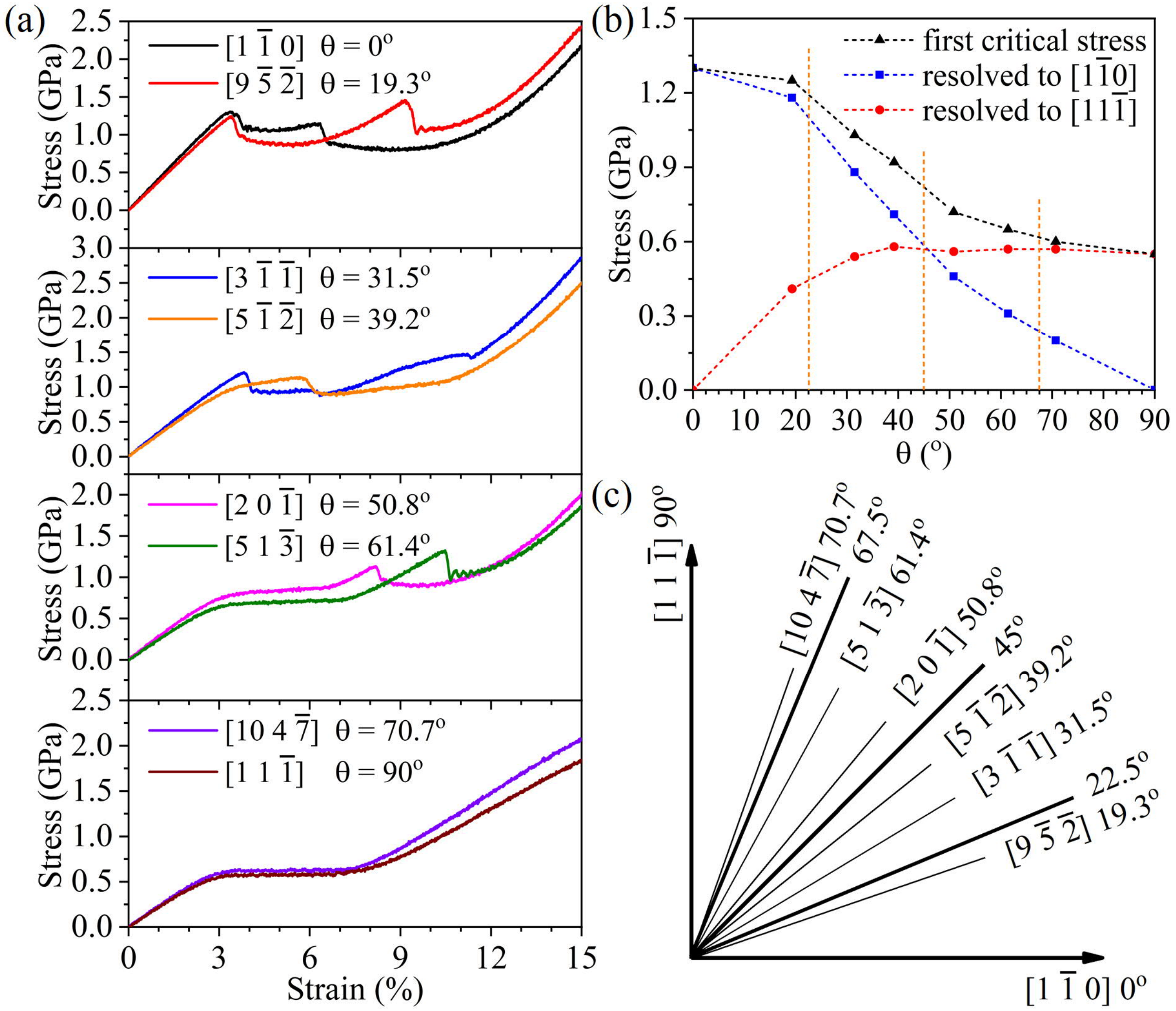
(a)
Stress (GPa)
[1 1̄ 0] θ = 0°
[9 5̄ 2̄] θ = 19.3°
[3 1̄ 1̄] θ = 31.5°
[5 1̄ 2̄] θ = 39.2°
[2 0 1̄] θ = 50.8°
[5 1 3̄] θ = 61.4°
[10 4 7̄] θ = 70.7°
[1 1 1̄] θ = 90°
0.0
0.5
1.0
1.5
2.0
2.5
3.0
0
3
6
9
12
15
Strain (%)
(b)
first critical stress
resolved to [11̄0]
resolved to [111̄]
Stress (GPa)
0.0
0.3
0.6
0.9
1.2
1.5
0
10
20
30
40
50
60
70
80
90
θ (°)
(c)
[1 1 1̄] 90°
[10 4 7̄] 70.7°
67.5°
[5 1 3̄] 61.4°
[2 0 1̄] 50.8°
45°
[5 1̄ 2̄] 39.2°
[3 1̄ 1̄] 31.5°
22.5°
[9 5̄ 2̄] 19.3°
[1 1̄ 0] 0°

Fig. 8

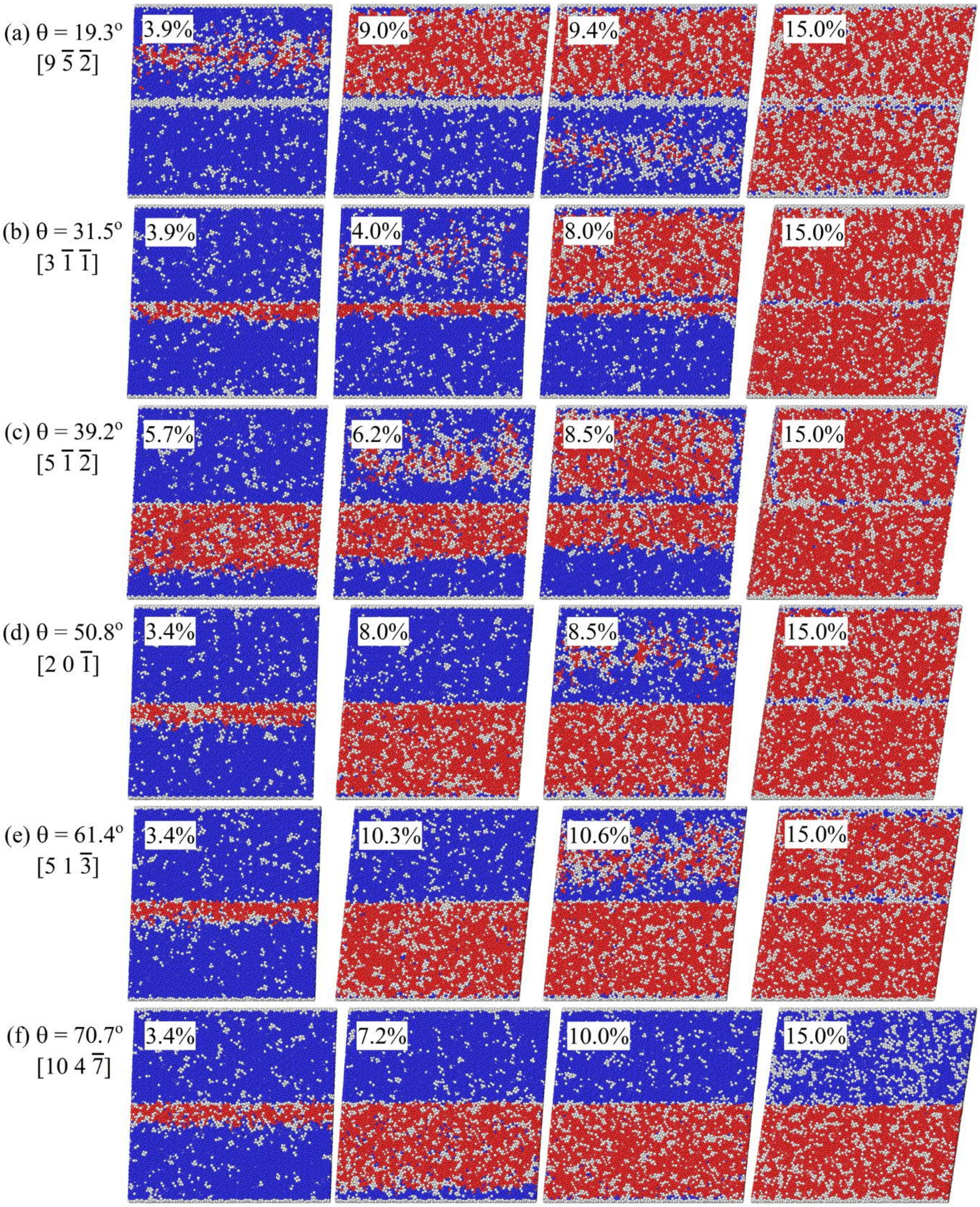
(a) θ = 19.3°
[9 $\bar{5}$ $\bar{2}$]
3.9%
9.0%
9.4%
15.0%
(b) θ = 31.5°
[3 $\bar{1}$ $\bar{1}$]
3.9%
4.0%
8.0%
15.0%
(c) θ = 39.2°
[5 $\bar{1}$ $\bar{2}$]
5.7%
6.2%
8.5%
15.0%
(d) θ = 50.8°
[2 0 $\bar{1}$]
3.4%
8.0%
8.5%
15.0%
(e) θ = 61.4°
[5 1 $\bar{3}$]
3.4%
10.3%
10.6%
15.0%
(f) θ = 70.7°
[10 4 $\bar{7}$]
3.4%
7.2%
10.0%
15.0%

Fig. 9

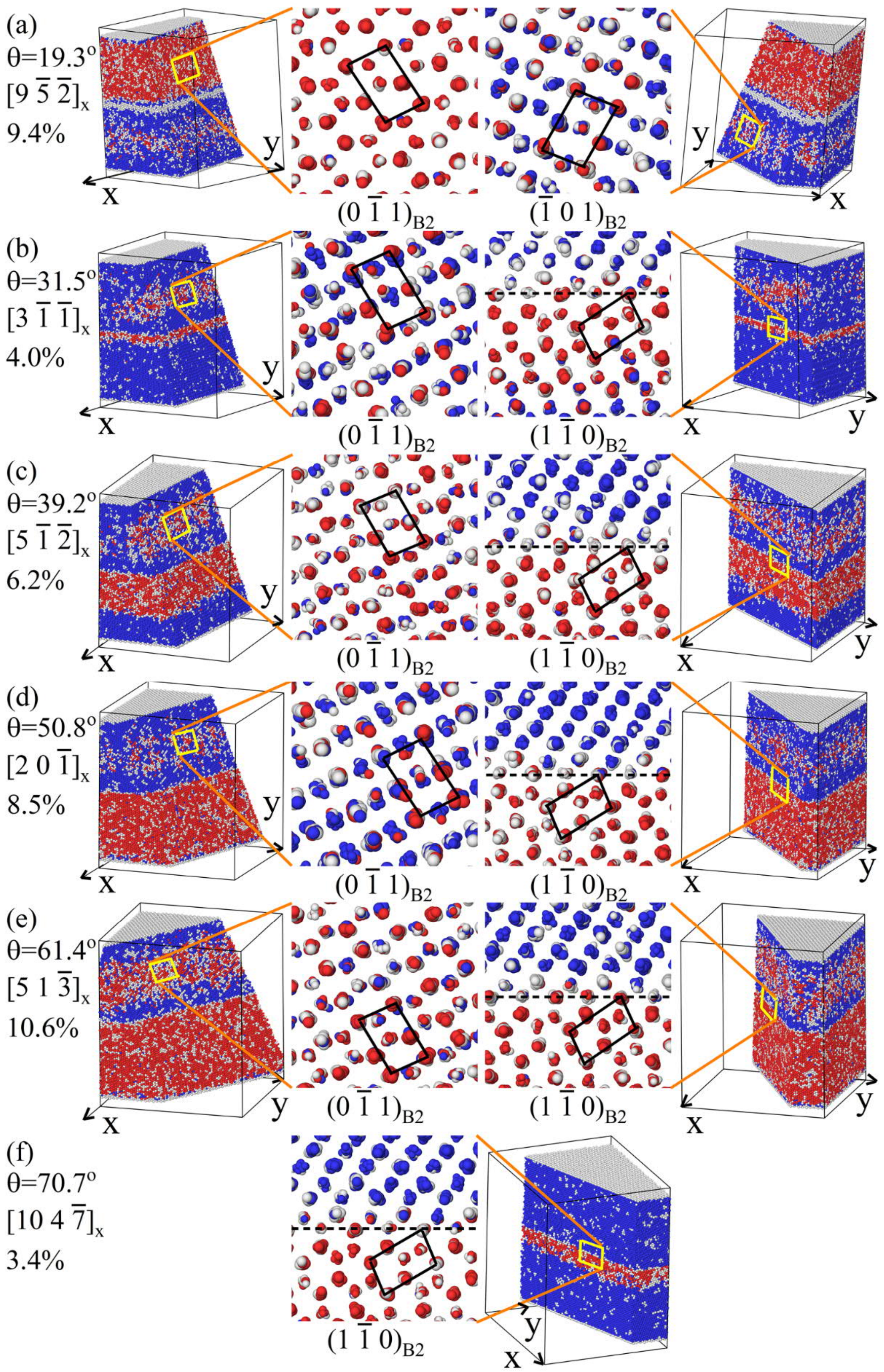
(a)
$\theta=19.3^{o}$
$[9\,\bar{5}\,\bar{2}]_x$
9.4%
$(0\,\bar{1}\,1)_{B2}$
$(\bar{1}\,0\,1)_{B2}$
(b)
$\theta=31.5^{o}$
$[3\,\bar{1}\,\bar{1}]_x$
4.0%
$(0\,\bar{1}\,1)_{B2}$
$(1\,\bar{1}\,0)_{B2}$
(c)
$\theta=39.2^{o}$
$[5\,\bar{1}\,\bar{2}]_x$
6.2%
$(0\,\bar{1}\,1)_{B2}$
$(1\,\bar{1}\,0)_{B2}$
(d)
$\theta=50.8^{o}$
$[2\,0\,\bar{1}]_x$
8.5%
$(0\,\bar{1}\,1)_{B2}$
$(1\,\bar{1}\,0)_{B2}$
(e)
$\theta=61.4^{o}$
$[5\,1\,\bar{3}]_x$
10.6%
$(0\,\bar{1}\,1)_{B2}$
$(1\,\bar{1}\,0)_{B2}$
(f)
$\theta=70.7^{o}$
$[10\,4\,\bar{7}]_x$
3.4%
$(1\,\bar{1}\,0)_{B2}$
x
y

Fig. 10